International Journal of Electrochemical Science 18 (2023) 100383

Contents lists available at ScienceDirect

International Journal of Electrochemical Science

journal homepage: www.editorialmanager.com/ijoes

Practical mechanochemical synthesis and electrochemical properties of Mn_3O_4 for use in supercapacitors

Lorena Cuéllar-Herrera [a], Elsa Arce-Estrada [a], Antonio Romero-Serrano [a,*], Daniella Esperanza Pacheco-Catalán [b], José Martín Baas-López [b], Josué López-Rodríguez [a]

[a] Instituto Politécnico Nacional-ESIQIE, UPALM, CDMX, C.P. 07738, Mexico
[b] Unidad de Energía Renovable, Centro de Investigación Científica de Yucatán, A.C. Carretera Sierra Papacal-Chuburná Puerto Km 5, Sierra Papacal, 97302 Mérida, Mexico

ARTICLE INFO

Keywords:
Mn_3O_4
Energy storage
Supercapacitor
Mechanochemical synthesis

ABSTRACT

A facile method to synthesize Mn_3O_4 crystalline powders for use in supercapacitor electrodes is reported. Specifically, the mechanochemical synthesis was carried out with high-energy ball milling and a short milling time of 1 h. The physicochemical properties of the resultant powders were characterized by XRD, Raman spectroscopy, SEM, and N_2 adsorption-desorption techniques. In addition, the electrochemical capabilities were tested in two different configurations: a three-electrode cell, and a symmetric supercapacitor (SSC) with a two-electrode arrangement. Cyclic voltammetry, electrochemical impedance spectroscopy, and galvanostatic charge-discharge were applied to the samples with both configurations. The Mn_3O_4 samples were synthesized from manganese chloride tetrahydrate and sodium peroxide with two molar ratios, 1:1 and 1:1.5. The samples showed excellent electrochemical stabilities of 99.7 % after 5000 charge-discharge cycles, and the highest electrochemical capacitance of 485 $F{\cdot}g^{-1}$ at 5 mV s^{-1} was observed for the sample prepared with a 1:1 ratio of reagents and used with the three-electrode configuration.

1. Introduction

A supercapacitor or electrochemical capacitor (EC) is a device capable of storing an electric charge. It consists of two electrodes that can be identical (made of the same material) for symmetrical supercapacitors (SSC) or different for asymmetrical supercapacitors (ASC). The assembly requires an electrolyte-soaked separator between the electrodes that prevents contact and is generally made of thin ion-permeable materials to transfer ionic charges within the cell. Depending on the charge storage mechanism, supercapacitors can be divided into electrochemical double-layer capacitors (EDLCs), electrochemical capacitors with pseudocapacitance, and hybrid electrochemical capacitors. Transition metal oxides, such as manganese oxide, show promise for use as electrodes in supercapacitors exhibiting pseudocapacitance [1–3].

Manganese oxides have different forms due to the multiple oxidation states of manganese. Among these oxides, Hausmannite-Mn_3O_4, has been attracting interest due to its high theoretical capacitance (up to 1400 $F{\bullet}g^{-1}$) [4] and for a wide range of applications, such as in catalysis, biosensors, and energy storage, especially for supercapacitors [5]. In addition, manganese oxides are economically and environmentally friendly and have been prepared by several methods. Fang et al. [6] reported Mn_3O_4 nanowires prepared by the colloidal method and used as electrode materials for supercapacitors. They reported a large specific capacitance of 433.1 $F{\cdot}g^{-1}$ at a current density of 0.5 $A{\cdot}g^{-1}$. Shah et al. [7] synthesized Mn_3O_4 nanoparticles via the hydrothermal method and attained a specific capacitance of 389 $F{\cdot}g^{-1}$ with 88.6 % capacity retention. Shunmugapriya et al. [8] prepared Mn_3O_4 by the coprecipitation method at room temperature and confirmed that it was an excellent material for supercapacitor applications.

Wang et al. [9] prepared Mn_3O_4 microspheres by the cathode glow discharge electrolysis (CGDE) plasma technique for high-capacitance supercapacitor electrode materials. They showed that the electrochemical properties of Mn_3O_4 included 360 $F{\cdot}g^{-1}$ at a 0.5 $A{\cdot}g^{-1}$ current density. Ismail et al. [10] synthesized pure Mn_3O_4 and Mn_3O_4/rGO hybrid nanocomposites by a sol-gel-based in situ reduction method and reported that the specific capacitances were 136 $F{\cdot}g^{-1}$ and 427 $F{\cdot}g^{-1}$ for these materials, respectively. Qi et al. [11] used an electrochemical

* Corresponding author.
E-mail address: romeroipn@hotmail.com (A. Romero-Serrano).

https://doi.org/10.1016/j.ijoes.2023.100383
Received 28 August 2023; Received in revised form 9 October 2023; Accepted 13 October 2023
Available online 14 October 2023

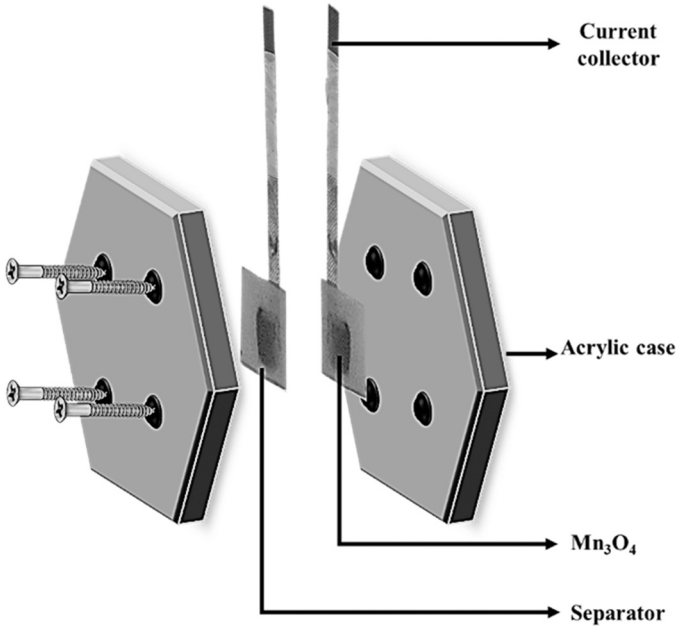

Fig. 1. Schematic showing the assembled structure of the SSC.

deposition method to prepare Mn_3O_4 from an $Mn(NO_3)_2$ solution and obtained a material with a 210 $F{\cdot}g^{-1}$ specific capacitance. Becker et al. [12] reported a mechanochemical synthesis of Mn_3O_4 at room temperature from MnO and Mn_2O_3.

The main pseudocapacitive process in manganese oxide-based electrodes involves interfacial redox reactions. This includes exchanges of both protons and metal cations in the electrolyte, leading to manganese oxidation state transitions ranging from Mn(III)/Mn(II), Mn(IV)/Mn (III), and Mn(VI)/Mn(II). The pseudocapacitive behavior of the manganese oxides depends on physical and chemical factors. There is a compromise between the degree of crystallinity and the specific surface area of the manganese oxide-based electrode; if the degree of crystallinity is too high, a very limited specific area is obtained, although the conductivity is increased. On the other hand, the high specific area and low degree of crystallinity diminish the conductivity of the material [13–15].

Exploring new synthesis and processing approaches for obtaining manganese oxide materials is expected to advance the state of the art for supercapacitor materials. In contrast to conventional solid-state reaction processes in which the reactions involve long processing time and high temperatures [16–19], reactive milling processes (especially those with high energies) accelerate the chemical reactions, making it possible to obtain the products more rapidly and at considerably lower temperatures [20–22]. The mechanochemical synthesis has not been widely explored for preparing manganese oxides; however, it shows versatility for obtaining materials for electrode supercapacitors [23,24].

In this study, fine Mn_3O_4 particles were prepared via the mechanochemical method by reacting manganese chloride and sodium peroxide at room temperature with the aim of investigating the effect of the ratio of the reagents on the structure and electrochemical properties by evaluating the capacitance of these materials. Structural characterizations and surface morphology analyses were carried out with X-ray diffraction (XRD) and scanning electron microscopy (SEM). The specific surface area was estimated with N_2 adsorption-desorption tests, and the electrochemical properties of Mn_3O_4 were investigated by cyclic voltammetry, electrochemical impedance spectroscopy, and cyclic stability tests.

2. Experimental

2.1. Synthesis of Mn_3O_4

The mechanochemical process was carried out with high-energy model Chemplex SpectroMill 1100 milling equipment. The container and balls used were made of zirconia to reduce contamination resulting from wear of the milling media during the process. The powdered reactant to ball weight ratio was 1:10.

All chemicals were of analytical grade. First, manganese chloride tetrahydrate ($MnCl_2{\cdot}4H_2O$) and sodium peroxide (Na_2O_2) were mixed in a zirconia milling vessel with different molar ratios of 1:1 and 1:5 and labeled MS1 and MS2, respectively. After milling for 60 min, the obtained powders were washed several times with deionized water and dried at 80 °C for 24 h.

2.2. Material characterization

The crystal structures of the prepared samples were determined by X-ray diffraction using a Bruker D2 PHASER X-ray diffractometer. The XRD patterns were recorded in the 2θ range 10°—80° using a source providing Cu Kα radiation (λ = 1.5406 Å). Raman spectra were recorded over the frequency range 100–3500 cm^{-1} with a Thermo Scientific DXR Raman microscope employing a laser emitting a wavelength of 630 nm. The specific surface area and pore volume measurements were carried out by the N_2 adsorption-desorption technique using Quanthachrome Autosorb IQ equipment. The obtained isotherms were analyzed with the Brunauer-Emmett Teller (BET) and Barrett—Joyner—Halenda (BJH) models. The sample morphology was obtained with a scanning electron microscope model JEOL JSM 6701 F.

2.3. Electrode fabrication

The working electrodes were prepared by forming an ethanol-based slurry and mixing in 30 wt% black carbon (Super P conductive, Alfa Aesar, UK), 10 wt% polytetrafluoroethylene (Sigma Aldrich, USA), and 60 wt% of Mn_3O_4. The prepared slurry was spread on a stainless-steel mesh (as a current collector) covering a mesh area of 1 cm^2 and then pressed at 3 tons for 5 min. The formed electrodes were soaked overnight in the electrolyte, 6 M KOH solution.

2.4. Electrochemical measurements

A three-electrode assembled system was first used to obtain the optimum material performance and then to assemble a symmetric supercapacitor (SSC) with a two-electrode configuration. The studies of the single electrodes in a three-electrode cell were carried out in a 6 M KOH electrolyte solution. A porous graphite bar of 0.5 mm diameter and 20 cm long was used as the counter electrode, and the synthesized Mn_3O_4 was used as the working electrode. Cyclic voltammetry was conducted at different scanning rates between 5 and 100 mV s^{-1} and over a potential window of —0.45–0.25 V versus SCE (saturated calomel electrode). Electrochemical impedance spectroscopy was carried out with a sine amplitude of ± 10 mV against OCP over a frequency range of 0.02 Hz—100 kHz, and a BioLogic Science Instruments potentiostat/galvanostat equipped with an impedance module was used to collect the data. The Z-Fit tool from EC-Lab VII.34 software was used to adjust the experimental curves and predict the equivalent circuits. The specific capacitances (Cs) of the electrodes were calculated with the following equation [7]:

$$C_S = \frac{1}{v \bullet m \bullet \Delta E} \bullet \int_{E_a}^{E_c} j \quad dE \tag{1}$$

where v is the scanning rate in V s^{-1}, ΔE is the potential window in V, m is the mass of the active material contained in the electrode in g and $\int_{E_a}^{E_c}$

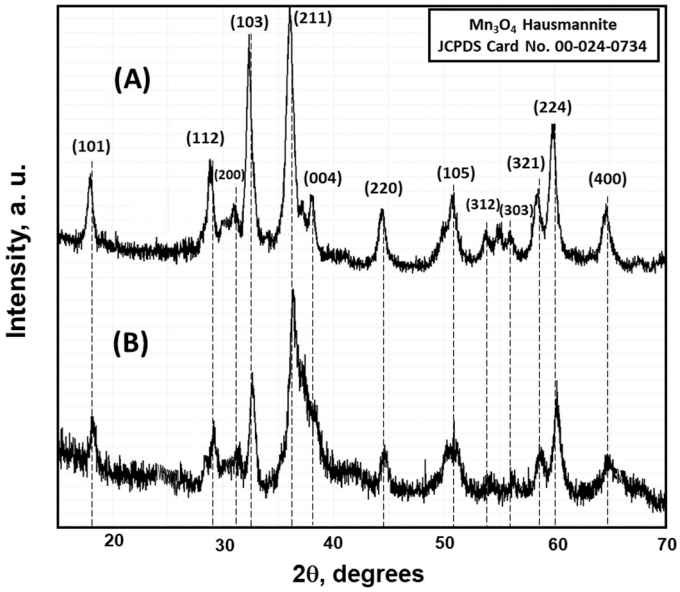

Fig. 2. XRD profiles of (A) MS1 and (B) MS2.

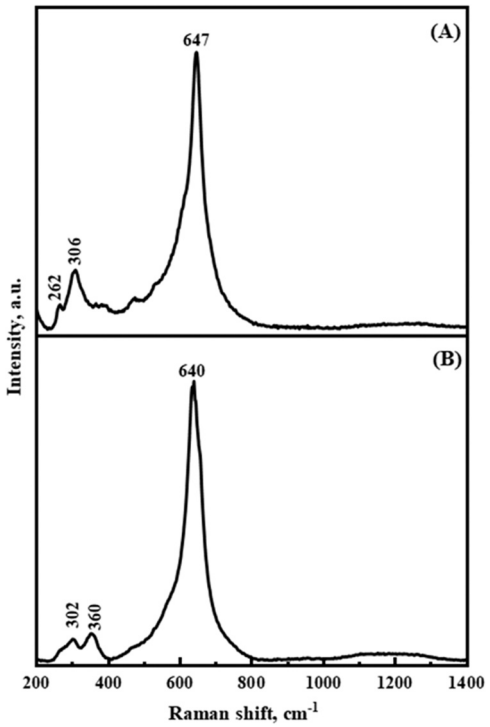

Fig. 3. Raman spectra of the manganese oxide (Mn_3O_4) powders; (A) MS1 and (B) MS2.

j dE is the total area obtained by the cyclic voltammograms in C.

The SSC cells were fabricated by assembling two Mn_3O_4 electrodes as the anode and cathode, which were separated by filter papers previously soaked in 6 M KOH in an acrylic case, as shown in Fig. 1.

The weight of each Mn_3O_4 slurry was approximately 5 mg, and it was deposited on a 1 cm^2 316 stainless steel mesh. The electrochemical performance was tested with cyclic voltammetry (CV), electrochemical impedance spectroscopy (EIS), and galvanostatic charge-discharge (GCD) techniques in 6 M KOH solutions. GCD testing was carried out at current densities of 50 mA g^{-1} in the same potential window used to CV (0–0.25 V). The materials were evaluated up to 5000 charges/

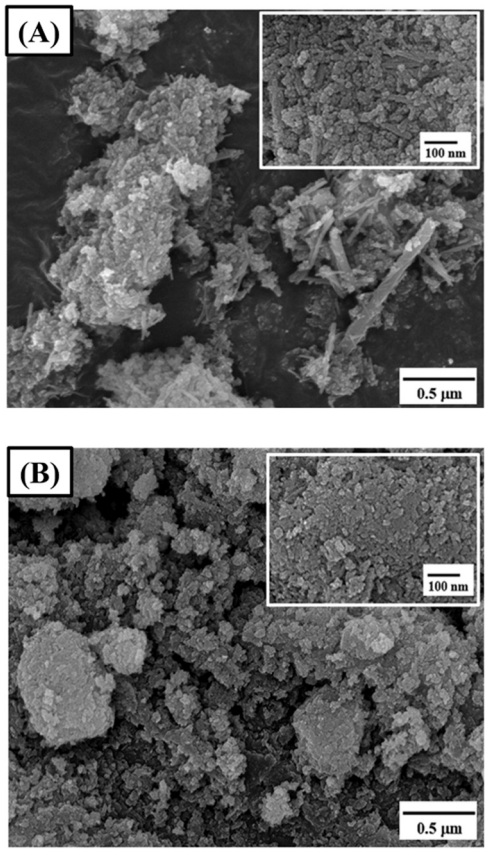

Fig. 4. SEM images of the samples; (A) MS1 and (B) MS2.

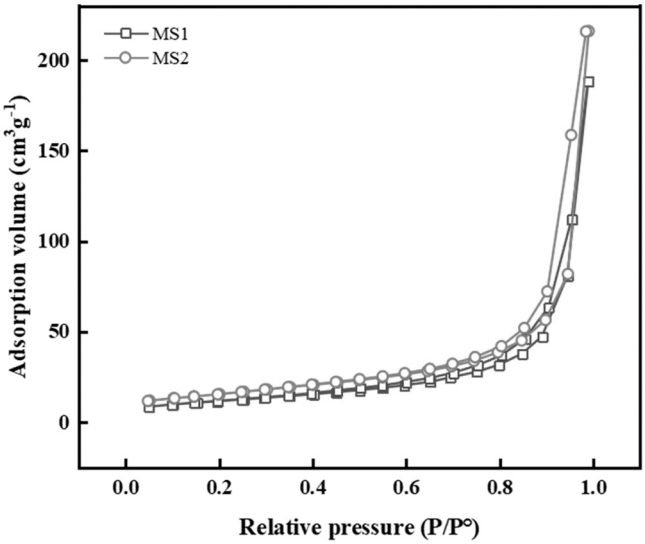

Fig. 5. N_2 adsorption-desorption isotherms of the samples.

Table 1
Specific surface areas and total pore volumes of the Mn_3O_4 samples.

Sample	Specific surface area (m^2 g^{-1})	Total pore volume (cm^3 g^{-1})	Average pore diameter (nm)
MS1	41.455	0.29	34.13
MS2	55.004	0.33	32.62

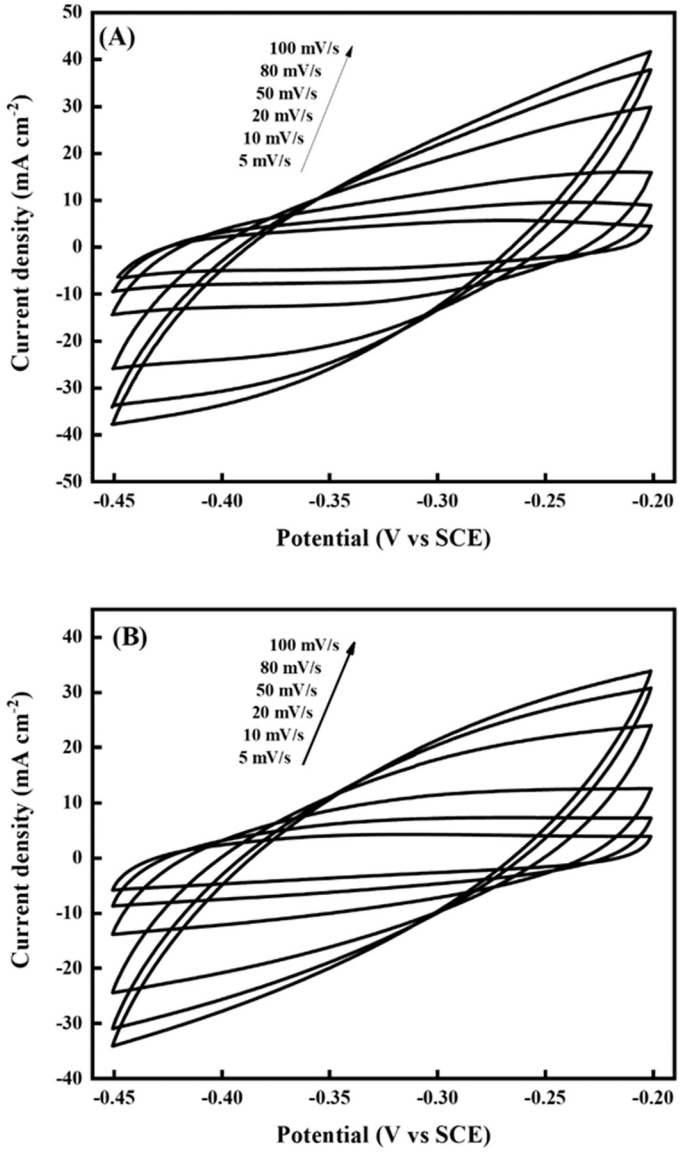

Fig. 6. Cyclic voltammograms of the prepared samples in three-electrode assembled systems; (A) MS1 and (B) MS2.

discharges cycles. The coulombic efficiency (CE) of cycle n is defined as the measured discharge capacity of cycle n ($C_{Dch(n)}$) over the preceding measured charge capacity ($C_{Ch(n)}$).

$$CE = \frac{C_{Dch(n)}}{C_{Ch(n)}}(100) \quad (2)$$

3. Results and discussion

3.1. Physicochemical properties of the as-synthesized Mn_3O_4 powders

Two Mn_3O_4 samples were synthesized with different amounts of the oxidizing agent (Na_2O_2). Reactions (3) and (4) are proposed for the syntheses of Mn_3O_4 with the 1:1 and 1:1.5 molar ratios of $MnCl_2$:Na_2O_2, respectively.

$$3[MnCl_2{\cdot}4H_2O_{(s)}] + 3Na_2O_{2(s)} \rightarrow Mn_3O_{4\,(s)} + 6NaCl_{\,(s)} + 12H_2O_{(l)} + O_{2\,(g)} \quad (3)$$

$$3[MnCl_2{\cdot}4H_2O_{(s)}] + 4{\cdot}5Na_2O_{2(s)} \rightarrow Mn_3O_{4\,(s)} + 6NaCl_{(s)} + 3NaOH_{(s)} + 10{\cdot}5H_2O_{(l)} + 1{\cdot}75O_{2(g)} \quad (4)$$

The sample labeled MS1 contained stoichiometric amounts of reagents in reaction (3), whereas the sample labeled MS2 was prepared with a 50 % excess of the oxidizing reagent used to form the Mn_3O_4 phase.

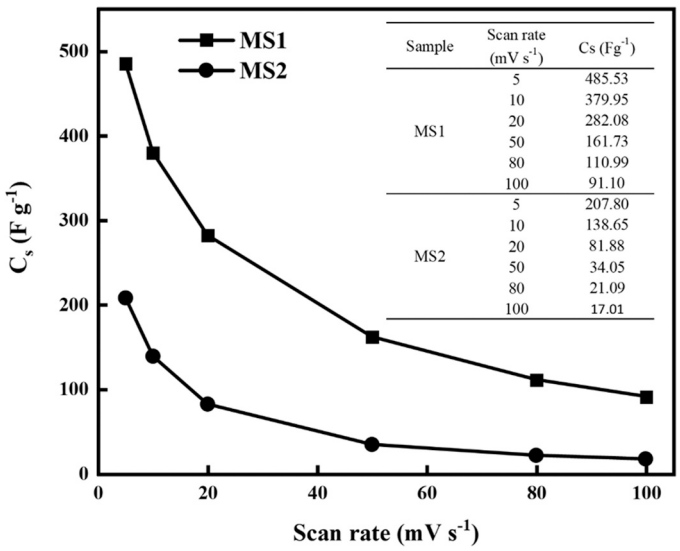

Sample	Scan rate (mV s^{-1})	Cs (Fg^{-1})
MS1	5	485.53
	10	379.95
	20	282.08
	50	161.73
	80	110.99
	100	91.10
MS2	5	207.80
	10	138.65
	20	81.88
	50	34.05
	80	21.09
	100	17.01

Fig. 7. Comparison of C_S vs. scan rate with the three-electrode assembled system.

The effect of the excess of Na_2O_2 can be explained as follows: according to the Debye-Hückel theory, the rate of supersaturation of solution increases when the Na^+ ions are increased which causes the solubility of the product increases (Mn^{2+} and Mn^{3+}). Therefore, a lower concentration of Na^+ ions is suitable for the formation of Mn_3O_4 nanoparticles. Similar results were obtained by Edrissi and Soleymani [25] during the preparation of magnetite by the oxidation of Fe^{2+} using Na_2O_2.

The crystalline phases of the synthesized powders were examined by X-ray diffraction. Fig. 2 shows the XRD patterns of the Mn_3O_4 obtained samples. In both samples, the diffraction peaks for the (101), (112), (200), (103), (211), (004), (220), (105), (312), (224), and (400) planes were indexed to the pure tetragonal phase of Hausmannite-Mn_3O_4 with a spinel structure (JCPDS Card No. 00-024-0734). The diffraction profile of the samples exhibits high-intensity peaks that indicate the high crystallinity of the Mn_3O_4. Results on the amount of the oxidizing agent reveal minor differences regarding their microstructural features. The estimated crystallite, based on the Sherrer formula, reveals values of 14 and 12 nm for samples MS1 and MS2, respectively. Obtaining crystalline and pure Mn_3O_4 in one step and short processing times confirmed the advantages of the ball milling-based process.

The Raman spectra of the Mn_3O_4 powders are shown in Fig. 3. The strongest peaks at 647 and 640 cm^{-1} for MS1 and MS2, respectively, were attributed to the A_{1g} Mn-O breathing vibration in the spinel structures ($MnMn_2O_4$), which confirmed the presence of divalent manganese in tetrahedral coordination sites of the Hausmannite-Mn_3O_4 phase [26]. The other two weak peaks located at 262 and 306 cm^{-1} for MS1 and 302 and 360 for MS2 were assigned to different vibrational modes involving octahedral and tetrahedral coordination by oxygen atoms [27].

The morphology was evaluated by SEM. Fig. 4 shows that the amount of oxidizing agent had an important effect on the morphological features of the materials. Nanorod-like particles were obtained from the stoichiometric 1:1 mol ratio of the reagents (sample MS1), and quasi-spherical particles with micrometer sizes were obtained with the non-stoichiometric 1:1.5 mol ratio of the reagents (sample MS2). We consider that by increasing the Na_2O_2 in the synthesis of sample MS2, the morphology of nanorods converted to Mn_3O_4 quasispheres by means of the accelerated nucleation growth in the reaction mixture.

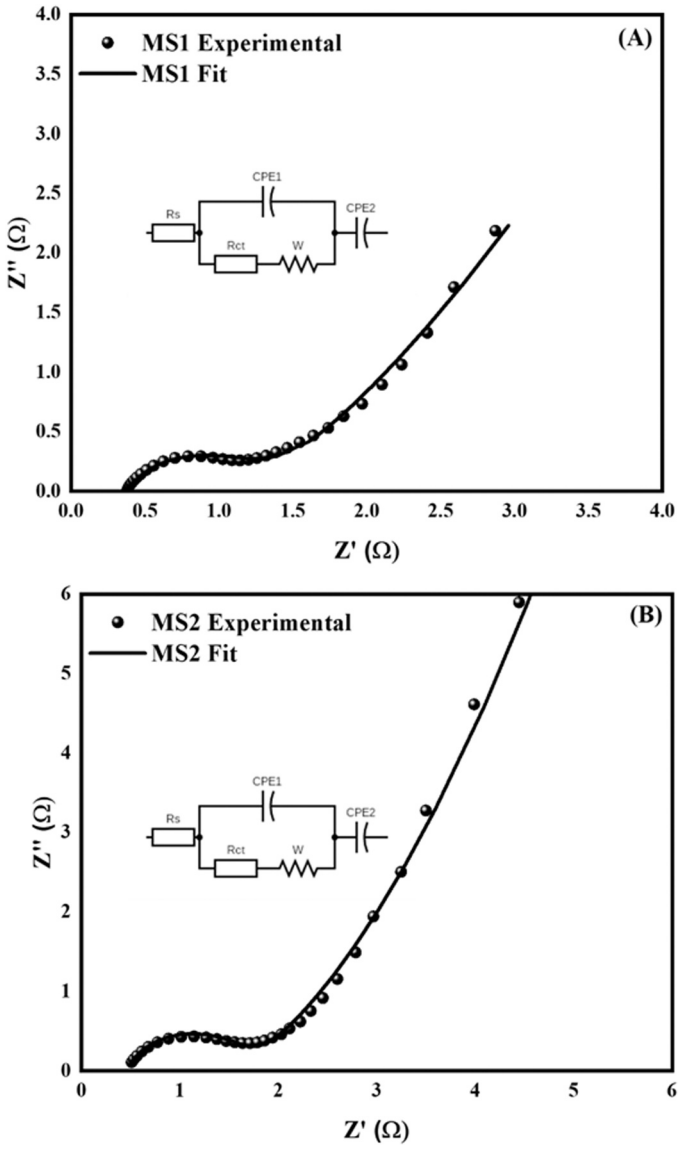

Fig. 8. Nyquist plots of (A) MS1 and (B) MS2 in a three-electrode cell.

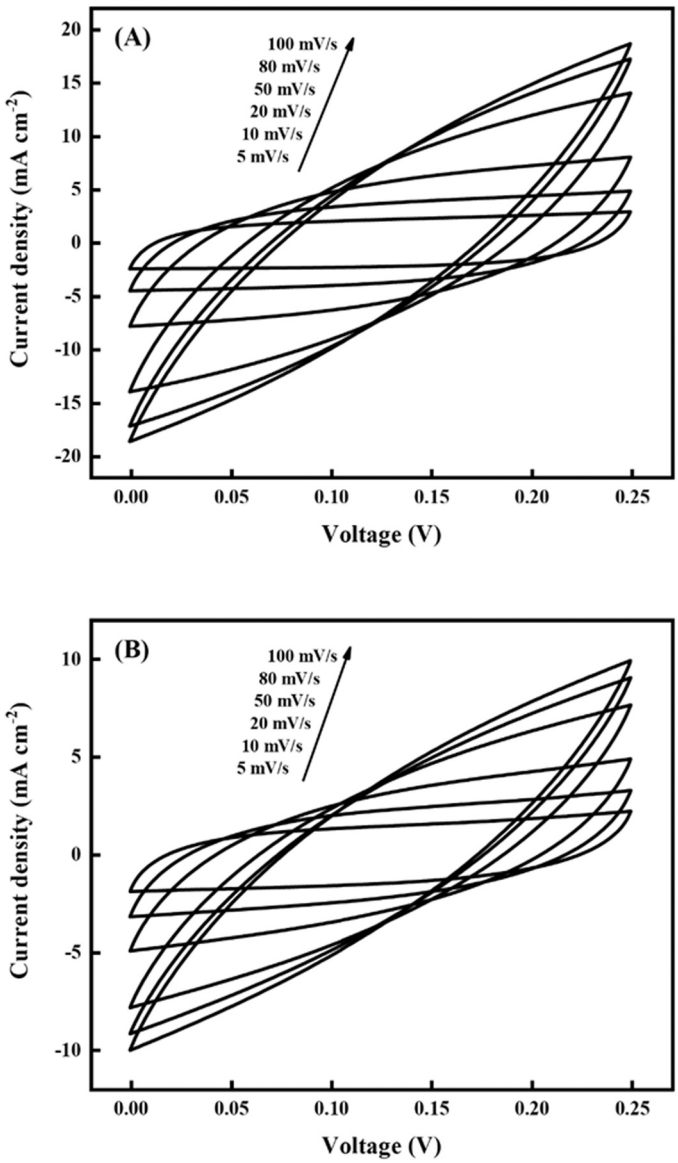

Fig. 9. Cyclic voltammograms of (A) MS1 and (B) MS2 in a two-electrode assembled system.

Table 2
Parameter values obtained by fitting the EIS diagrams.

Sample	R_s (Ω)	CPE_1		R_{ct} (Ω)	CPE_2		W (Ω $s^{-1/2}$)
		F $s^{(a-1)}$	n_1		F $s^{(a-1)}$	n_2	
MS1	0.371	0.0045	0.690	0.915	8.476	0.595	2.221
MS2	0.466	0.00301	0.771	1.266	1.012	1.0	1.552

Fig. 5 shows the N_2 adsorption-desorption isotherms of the samples prepared by the mechanochemical synthesis. Both exhibited the type IV hysteresis loops H3 of the IUPAC classification, indicating the formation of mesoporous solids [28]. The calculated surface areas and average pore sizes are shown in Table 1. The surface areas were 41.4 $m^2\ g^{-1}$ and 55 $m^2\ g^{-1}$ for the MS1 and MS2 samples, respectively.

3.2. Electrochemical measurements

3.2.1. Three-electrode configuration

CV with different scan rates and EIS techniques were applied in a three-electrode cell to evaluate the samples' electrochemical performance and specific capacitances (Cs). Fig. 6 shows CV profiles obtained at —0.45–0.25 V vs SCE with a KOH electrolyte and different scan rates. The CV profiles of both samples were quasi-rectangular, exhibiting nearly symmetrical shapes and showing no peaks in the reduction and oxidation zones; this behavior is well-known for manganese oxide-based electrodes and is attributed to their natural capacitance. Fig. 7 shows the specific capacitances obtained at different scan rates, which were higher at lower scan rates. The C_S results obtained at 5 mV s^{-1} with Eq. 1 were 485 and 207 $F{\cdot}g^{-1}$ for samples MS1 and MS2, respectively. This occurred because, at slow scan rates, the cations coming from the electrolyte (K^+ in this case) had more opportunity to interact at the electrode/electrolyte interface as well as in the bulk electrode. This enabled the diffusion of more cations into the active sites of the electrode material, leading to reversible oxidation-reduction reactions and intercalation-deintercalation reactions of the cations. These processes were the following surface Faradaic and bulk Faradaic reactions [7]:

$$(MnO_2)_{surface} + C^+ + e^- \leftrightarrow (MnOOC)_{surface} \quad (5)$$

$$MnO_2 + C^+ + e^- \leftrightarrow MnOOC \quad (6)$$

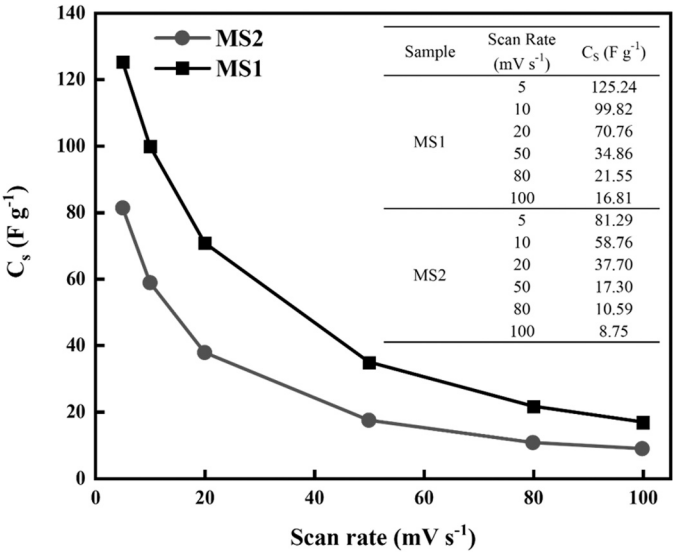

Sample	Scan Rate (mV s^{-1})	C_S (F g^{-1})
MS1	5	125.24
	10	99.82
	20	70.76
	50	34.86
	80	21.55
	100	16.81
MS2	5	81.29
	10	58.76
	20	37.70
	50	17.30
	80	10.59
	100	8.75

Fig. 10. Comparison of C_S vs. scan rate in a two-electrode assembled system (SSC).

The cations in the electrolyte interacted only at the electrode/electrolyte interface at high scan rates since the potassium cations did not reach the less accessible electrochemically active sites [7].

Despite MS1 showing a lower specific surface area than MS2, it has been reported that other microstructural features i.e., particle size, pore size, and morphology play a significant role in the specific capacitance [29]. González et al. [30] reported that the microstructure controls the cycling stability, whereas the chemical hydrated state controls the specific capacitance. The results of the present work showed that the particle sizes in the nanometric range, rod-like morphology, and the open pore size of about 34 nm exhibited by the MS1 sample, resulted in an excellent specific capacitance of 485 F g^{-1}. Moreover, the defects chemistry of the system could be influenced by the synthesis conditions as the amount of oxidizing agent must be changed on the ratio of Mn^{2+}/Mn^{3+} in the material therefore changing the electrochemical behavior. Further efforts will be focused on this regard.

Fig. 8 shows the Nyquist plots obtained with electrochemical impedance spectroscopy (EIS). The plots for both samples displayed small semicircles in the high-frequency region, indicating the operation of redox reactions due to the pseudocapacitive nature of the Mn_3O_4, and a nearly vertical line in the low-frequency region, indicating capacitive behavior [7].

An equivalent electrical circuit (inset in Fig. 8) was used to understand the charge transfer phenomena; the fitted plots are shown with a solid line in the Nyquist plots. The selected equivalent electrical circuit comprises R_Ω, R_{ct}, W, CPE_1 and CPE_2, where R_Ω is the combined resistance including the internal resistance, contact resistance, and electrolyte ionic resistance, R_{ct} is the charge transfer resistance, W is the Warburg impedance. CPE_1 is the constant phase element that corresponds to double-layer capacitance. The CPE_2 is a low-frequency constant phase element that accounts for the low-frequency spike observed in the impedance plot [31]. The fit of impedance plots was carried out using the Z-tool fit program and the obtained data are shown in Table 2. The values calculated for R_s were as low as 0.3 Ω and 0.4 Ω for MS1 and MS2, respectively, which indicated excellent contact between the material and the current collector. The R_{ct} values were 0.8 Ω for MS1 and 1.2 Ω for MS2, indicating low internal resistance for both materials; together with the high specific capacitance obtained by CV, these materials have potential for use in SSCs.

3.2.2. SSC with a two-electrode arrangement

To determine the electrochemical capabilities of the samples in a supercapacitor device, an SSC with a two-electrode arrangement was constructed with a Mn_3O_4-based anode and cathode. Fig. 9 shows the CV curves obtained exhibiting quasi-rectangular and symmetrical shapes and the absence of peaks; this suggested the predominant capacitive behavior of the Mn_3O_4, as seen with the three-electrode system. Furthermore, Fig. 10 shows that maximum C_S values of 125 and 81 F·g^{-1} were obtained for samples MS1 and MS2, respectively. The Cs values of sample MS1 were higher than those of sample MS2, consistent with the tendency described previously, which was attributed to particle size and morphology differences.

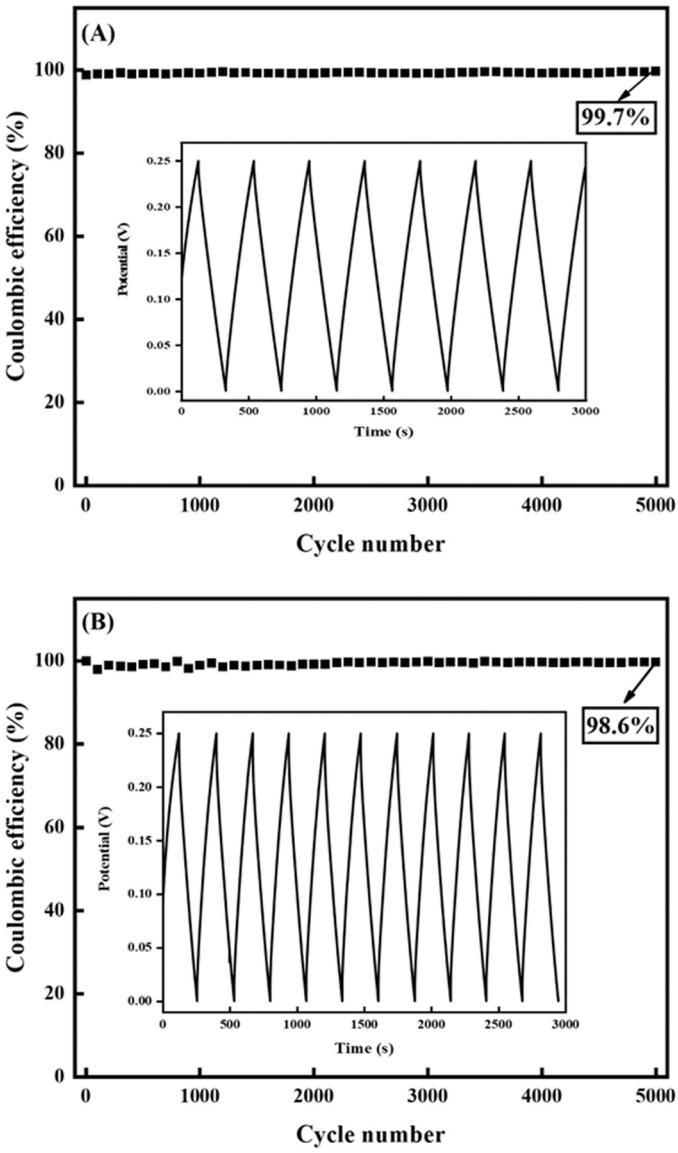

Fig. 11. Cycling performance of (A) MS1 and (B) MS2 after 5000 cycles in a two-electrode cell.

Fig. 11 shows the cycling stabilities of the samples studied with the GCD technique at 0.05 A·g^{-1}; samples MS1 and MS2 exhibited stable charge-discharge cycling and outstanding coulombic efficiency rates of 99.7 % and 98.6 %, respectively, after 5000 cycles. The higher coulombic efficiency of sample MS1 can be ascribed to the lower internal resistance, shorter ion transport distances, and better electroactive surface [32]. This confirmed the stabilities of the electrodes during long-term cycling.

The current collector, on which material is deposited, affects the performance of supercapacitor cells. Stainless steel mesh, nickel foil, and carbon cloth fiber are common current collector bases. We use stainless

Table 3
Electrochemical properties of the Mn_3O_4 electrodes obtained with different methods. Results are from the three-electrode mode.

Nature of Mn_3O_4	Method	Electrolyte	Specific capacitance (F g^{-1})	Cycling stability	Reference
Powder	Hydrothermal	2 M KCl	148	400	[34]
Powder	Hydrothermal	1 M Na_2SO_4	170	1500	[35]
Powder	Precipitation	1 M Na_2SO_4	247	2000	[36]
Film	Ultrasonic irradiation	6 M KOH	296	1000	[37]
Film	Coprecipitation	2 M KOH	202	—	[38]
Film	Sol-gel	2 M KOH	285	—	[38]
Film	Electrospinning	2 M KOH	150	—	[39]
Powder	Mechanosynthesis	6 M KOH	485	5000	This work

steel mesh because has high mechanical strength, high electrical conductivity, porosity, and enhanced electrochemical affinity to be used as a base material for supercapacitor electrodes. Besides, stainless steel mesh-based electrodes exhibit superior energy capability than nickel foil or carbon cloth as current collectors [33]. This could be attributed to the higher specific surface area ensuring the larger electroactive material/current-collector interfaces to reduce the interfacial resistance. The galvanostatic charge-discharge test was performed appropriately at the relatively low current density of 0.05 A g^{-1}.

Finally, Table 3 summarizes the essential results for different methods used to prepare Mn_3O_4 materials and their electrochemical capabilities as supercapacitor electrodes. The results reported in the literature, and shown in Table 3, correspond to the measurements under the three-electrode mode. The Mn_3O_4 electrodes prepared in this work exhibited remarkable behaviors. Although little information was available on the use of mechanical methods in Mn_3O_4 syntheses, this work confirms that they could be excellent options for obtaining high-performance supercapacitor electrodes.

4. Conclusions

The mechanochemical synthesis formed crystalline and pure Hausmannite-Mn_3O_4, prepared with milling times as short as 1 h. Microstructural changes were observed depending on the amount of oxidizing agent (Na_2O_2) used; a stoichiometric amount of Na_2O_2 was preferred to prepare nanometer-sized particles. XRD, Raman spectroscopy, and N_2 absorption/desorption evidenced these changes. The CV, EIS, and GCD electrochemical analyses showed that the samples had the characteristic pseudocapacitive behavior of manganese oxides, and high specific capacitance values were obtained. Sample MS1 showed the best electrochemical performance with a C_S value of 485 F g^{-1} at a scan rate of 5 mV·s^{-1} and outstanding coulombic efficiency of 99.7 % after 5000 charge/discharge cycles, which makes this a very promising material for use electrodes for supercapacitors.

Declaration of Competing Interest

The authors declare that they have no known competing financial interests or personal relationships that could have appeared to influence the work reported in this paper. This study was funded by CONACYT grant number A1-S 9692. The authors declare that they have no conflict of interest.

Acknowledgments

The authors wish to thank the National Council for Science and Technology (CONAHCYT), National Polytechnic Institute (IPN) and the Researcher National System (SNI) for the support of this research.

References

[1] W. Zhao, Y. Zeng, Y. Zhao, X. Wu, Recent advances in metal-organic framework-based electrode materials for supercapacitors: a review, J. Energy Storage 62 (2023), 106934, https://doi.org/10.1016/j.est.2023.106934.
[2] M. Mustaqeem, G.A. Naikoo, M. Yarmohammadi, M.Z. Pedram, H. Pourfarzad, R. A. Dar, S.A. Taha, I.U. Hassan, M.Y. Bat, Y.F. Chen, Rational design of metal oxide based electrode materials for high performance supercapacitors – a review, J. Energy Storage 55 (2022), 105419, https://doi.org/10.1016/j.est.2022.105419.
[3] B.B. Sahoo, V.S. Pandey, A.S. Dogonchi, P.K. Mohapatra, D.N. Thatoi, N. Nayak, M. K. Nayak, A state-of-art review on 2D material-boosted metal oxide nanoparticle electrodes: supercapacitor applications, J. Energy Storage 65 (2023), 107335, https://doi.org/10.1016/j.est.2023.107335.
[4] W. Wei, X. Cui, W. Chen, D.G. Ivey, Manganese oxide-based materials as electrochemical supercapacitor electrodes, Chem. Soc. Rev. 40 (2011) 1697–1721, https://doi.org/10.1039/C0CS00127A.
[5] A. Kanwade Lichchhavi, P.M. Shirage, A review on synergy of transition metal oxide nanostructured materials: Effective and coherent choice for supercapacitor electrodes, J. Energy Storage 55 (2022), 105692, https://doi.org/10.1016/j.est.2022.105692.
[6] Q. Fang, M. Sun, X. Ren, B. Cao, W. Shen, Z. Li, Y. Fu, Ultrafine Mn_3O_4 nanowires synthesized by colloidal method as electrode materials for supercapacitors with a wide voltage range, J. Energy Storage 44 (2021), 103260, https://doi.org/10.1016/j.est.2021.103260.
[7] H.U. Shah, F. Wang, A.M. Toufiq, S. Ali, Z.U.H. Khan, Y. Li, J. Hu, K. He, Electrochemical properties of controlled size Mn_3O_4 nanoparticles for supercapacitor applications, J. Nanosci. Nanotechnol. 18 (2018) 719–724, https://doi.org/10.1166/jnn.2018.14644.
[8] B. Shunmugapriya, T. Vijayakumar, Investigation on the synthesis of Mn_3O_4 nanoparticles embedded on nano rods as an electrode material for supercapacitor application, Inorg. Chem. Commun. 146 (2022), 110179, https://doi.org/10.1016/j.inoche.2022.110179.
[9] B. Wang, J. Yu, Q. Lu, Z. Xiao, X. Ma, Y. Feng, Preparation of Mn_3O_4 microspheres via glow discharge electrolysis plasma as a high-capacitance supercapacitor electrode material, J. Alloy Compd. 926 (2022), 166775, https://doi.org/10.1016/j.jallcom.2022.166775.
[10] M.M. Ismail, S. Hemaanandhan, D. Mani, M. Arivanandhan, G. Anbalagan, R. Jayavel, Facile preparation of Mn_3O_4/rGO hybrid nanocomposite by sol–gel in situ reduction method with enhanced energy storage performance for supercapacitor applications, J. Sol. -Gel Sci. Technol. 93 (2020) 703–713, https://doi.org/10.1007/s10971-019-05184-z.
[11] Z. Qi, A. Younis, D. Chu, S. Li, A facile and template-free one-pot synthesis of Mn_3O_4 nanostructures as electrochemical supercapacitors, Nano-Micro Lett. 8 (2016) 165–173, https://doi.org/10.1007/s40820-015-0074-0.
[12] D. Becker, M. Klos, G. Kickelbick, Mechanochemical synthesis of Mn_3O_4 nanocrystals and their lithium intercalation capability, Inorg. Chem. 58 (2019) 15021–15024, https://doi.org/10.1021/acs.inorgchem.9b02429.
[13] T. Brousse, M. Toupin, R. Dugas, L. Athouël, O. Crosnier, D. Bélanger, Crystalline MnO_2 as possible alternatives to amorphous compounds in electrochemical supercapacitors, J. Electrochem Soc. 153 (2006) A2171, https://doi.org/10.1149/1.2352197.
[14] F. Liao, X. Han, D. Cheng, Y. Zhang, X. Han, C. Xu, H. Chen, MnO_2 hierarchical microspheres assembled from porous nanoplates for high-performance supercapacitors, Ceram. Int 45 (2019) 1058–1066, https://doi.org/10.1016/j.ceramint.2018.09.285.
[15] K. Chen, D. Xue, Searching for electrode materials with high electrochemical reactivity, J. Mater. 1 (2015) 170–187, https://doi.org/10.1016/j.jmat.2015.07.001.
[16] X. Bai, X. Tong, Y. Gao, W. Zhu, C. Fu, J. Ma, T. Tan, C. Wang, Y. Luo, H. Sun, Hierarchical multidimensional MnO_2 via hydrothermal synthesis for high performance supercapacitors, Electro Acta 281 (2018) 525–533, https://doi.org/10.1016/j.electacta.2018.06.003.
[17] X. Zhang, W. Yang, J. Yang, D.G. Evans, Synthesis and characterization of α-MnO_2 nanowires: Self-assembly and phase transformation to β-MnO_2 microcrystals, J. Cryst. Growth 310 (2008) 716–722, https://doi.org/10.1016/j.jcrysgro.2007.11.113.
[18] T.D. Xiao, E.R. Strutt, M. Benaissa, H. Chen, B.H. Kear, Synthesis of high active-site density nanofibrous MnO_2-base materials with enhanced permeabilities, Nanostruct. Mater. 10 (1998) 1051–1061, https://doi.org/10.1016/S0965-9773(98)00137-8.
[19] C. Liu, J. Wang, J. Tian, L. Xiang, Synthesis and surface characterization of nanostructures, J. Nanomater. 2013 (2013), 389634, https://doi.org/10.1155/2013/389634.
[20] K.J. Ardila-Fierro, J.G. Hernández, Sustainability assessment of mechanochemistry by using the twelve principles of green chemistry, ChemSusChem 14 (2021) 2145–2162, https://doi.org/10.1002/cssc.202100478.

[21] S.L. James, et al., Mechanochemistry: opportunities for new and cleaner synthesis, Chem. Soc. Rev. 41 (2012) 413–447, https://doi.org/10.1039/C1CS15171A.
[22] T. Tsuzuki, Mechanochemical synthesis of metal oxide nanoparticles, Commun. Chem. 4 (2021), 143, https://doi.org/10.1038/s42004-021-00582-3.
[23] R.E.A. Ngida, M.F. Zawrah, R.M. Khattab, E. Heikal, Utilization of leached MnO_2 for the mechanosynthesis of nano LaxCa1-xMnO_3 and LaxSr1-xMnO_3: sinterability and properties, Ceram. Int 46 (2020) 3433–3442, https://doi.org/10.1016/J.CERAMINT.2019.10.056.
[24] I. Antunes, L.C.M. Ruivo, L.A.C. Tarelho, A.A. Yaremchenko, A.V. Kovalevsky, J. R. Frade, $MnFe_2O_4$-based spinels by mechanochemical and thermochemical reaction of siderite and MnO_2 powder mixtures, Ceram. Int 49 (2023) 19495–19504, https://doi.org/10.1016/J.CERAMINT.2023.03.084.
[25] M. Edrissi, M. Soleymani, Preparation of magnetite nanoparticles by partial oxidation of Fe^{2+} using aqueous Na_2O_2, Synth. React. Inorg. M. 42 (2012) 935–939, https://doi.org/10.1080/15533174.2011.652277.
[26] D. Lan, et al., Synthesis, characterization and microwave transparent properties of Mn_3O_4 microspheres, J. Mater. Sci: Mater. Electro 30 (2019) 8771–8776, https://doi.org/10.1007/s10854-019-01201-7.
[27] F. Buciuman, F. Patcas, R. Craciun, D.R.T. Zahn, Vibrational spectroscopy of bulk and supported manganese oxides, Phys. Chem. Chem. Phys. 1 (1999) 185–190, https://doi.org/10.1039/a807821a.
[28] K.S.W. Sing, D.H. Everett, R.A.W. Haul, L. Moscou, R.A. Pierotti, J. Rouquerol, T. Siemieniewska, Reporting physisorption data for gas/solid systems with Special Reference to the determination of surface area and porosity, Pure Appl. Chem. 57 (1985) 603–619, https://doi.org/10.1351/pac198557040603.
[29] X. Yang, Y. Wang, H. Xiong, Y. Xia, Interfacial synthesis of porous MnO_2 and its application in electrochemical capacitor, Electrochem Acta 53 (2007) 752–757, https://doi.org/10.1016/j.electacta.2007.07.043.
[30] A. González, E. Goikolea, J.A. Barrena, R. Mysyk, Review on supercapacitors: technologies and materials, Renew. Sust. Energ. Rev. 58 (2016) 1189–1206, https://doi.org/10.1016/j.rser.2015.12.249.
[31] P.N. García-Hernández, J.M. Baas-López, T. Toledano-Thompson, R. Valdez-Ojeda, D. Pacheco-Catalán, Revalorization of pleurotus djamor fungus culture: fungus-derived carbons for supercapacitor application, Sustainability 13 (2021) 10765, https://doi.org/10.3390/su131910765.
[32] S.K. Meher, G.R. Rao, Enhance activity of microwave synthesized hierarchical MnO2 for high performance supercapacitor applications, J. Power Sources 215 (2012) 317–328, https://doi.org/10.1016/j.jpowsour.2012.04.104.
[33] A. Alimi, I.B. Assaker, J. Mozaryn, D. Ávila-Brande, E. Castillo-Martínez, R. Chtourou, Electrochemical synthesis of MnO2/NiO/ZnO trijunction coated stainless steel substrate as a supercapacitor electrode and cyclic voltammetry behavior modeling using artificial neural network, Int. J. Energy Res (2022) 1–17, doi: 10.100/er.8380.
[34] M. Fang, X. Tan, M. Liu, S. Kang, X. Hu, L. Zhang, Low-temperature synthesis of Mn_3O_4 hollow-tetrakaidecahedrons and their application in electrochemical capacitors, CrystEngComm 13 (2011) 4915–4920, https://doi.org/10.1039/c1ce05337j.
[35] T.-H. Wu, et al., Charge storage mechanism of activated manganese oxide composites for pseudocapacitors, J. Mater. Chem. A Mater. 3 (2015) 12786–12795, https://doi.org/10.1039/C5TA03334A.
[36] W. Ma, Y. Feng, L. Wang, J. Xue, H. Cui, Tailoring the size and electrochemical performance of Mn_3O_4 nanoparticles by controlling the precipitation process, J. Sol. -Gel Sci. Technol. 80 (2016) 326–332, https://doi.org/10.1007/s10971-016-4107-z.
[37] R. Tholkappiyan, A.N. Naveen, K. Vishista, F. Hamed, Investigation on the electrochemical performance of hausmannite Mn_3O_4 nanoparticles by ultrasonic irradiation assisted co-precipitation method for supercapacitor electrodes, J. Taibah Univ. Sci. 12 (2018) 669–677, https://doi.org/10.1080/16583655.2018.1497440.
[38] B.J. Rani, M. Ravina, G. Ravi, S. Ravichandran, V. Ganesh, R. Yuvakkumar, Synthesis and characterization of hausmannite (Mn_3O_4) nanostructures, Surf. Interfaces 11 (2018) 28–36, https://doi.org/10.1016/j.surfin.2018.02.007.
[39] J. Bhagwan, K.L. Yadav, Y. Sharma, Nanofiber of Mn_3O_4: Fabrication and application as supercapacitor electrode, AIP Conf. Proc. (2015), 050188, https://doi.org/10.1063/1.4917829.